



Design and preliminary test of tritiated water online detector system based on plastic scintillators

Chun-Hui Dong¹ · Kai-Yong Liao¹ · Rui-Yang Xu¹ · Hong-Wu Liu¹ · Qing-Xian Zhang¹

Received: 2 July 2022 / Revised: 22 August 2022 / Accepted: 27 August 2022 / Published online: 11 October 2022

© The Author(s), under exclusive licence to China Science Publishing & Media Ltd. (Science Press), Shanghai Institute of Applied Physics, the Chinese Academy of Sciences, Chinese Nuclear Society 2022

Abstract In this study, an online detector system based on plastic scintillators is designed to monitor the activity of tritiated water in the liquid effluents of nuclear power plants. The feasibility of the detector is verified via simulation on Geant4, and the optimal detector structure size is determined. A back-end electronics system is designed, and an experimental measurement platform for β -rays based on a ^{40}KCl solution is constructed. Thirteen ^{40}KCl solutions with different activities ranging from 10 to 4500 Bq/L are measured, and 1300 V is determined as the optimal operating high voltage of the photomultiplier tubes. A linear fit is performed in 10-min counts, and the maximum linear goodness of fit (R^2) achieved is 0.9992. Long-term stability measurements are performed for two detectors, one filled with air and the other with a ^{40}KCl solution exhibiting an activity of 2000 Bq/L. The relative deviation of the counts of the detector system every 10 min is 0.998% when the ^{40}KCl solution is used, and the maximum Gaussian R^2 of the counts is 0.9849.

Keywords Tritiated water · Geant4 · Plastic scintillator · Electronics system

1 Introduction

Tritium, which is an isotope of hydrogen that comprises one neutron and two protons, is a pure β -decaying radionuclide that emits β -rays with a maximum energy of 18.6 keV and an average energy of 5.7 keV when decaying; its half-life is 12.43 years [1, 2]. Tritium typically appears in the form of tritium gas and tritiated water, which primarily affect human health through internal irradiation owing to the low-energy of β -rays released from tritium decay and the inability of tritium to penetrate the human skin [3]. Once ingested by the human body, tritium is rapidly absorbed and utilized via its entry into the bloodstream from the gastrointestinal tract or alveoli. Within minutes, tritium appears in body fluids, organs, and other tissues at varying concentrations. It is uniformly distributed in all biological fluids within 1–2 h, thus causing irreversible damage to human tissue cells [4]. Currently, owing to the prohibition of explosion from nuclear weapon tests, tritiated water is primarily generated in the water coolant, and a moderator and is stored in the liquid effluent from the primary circuit of nuclear power plants. Many countries impose legal restrictions on the maximum activity of tritiated water discharged in liquid effluents from nuclear power plants [5, 6]. In addition, owing to the necessity to continuously use liquid water to cool down reactors after the Fukushima nuclear accident in Japan, a significant amount of radioactive wastewater has been generated. Previously, the Japanese government decided to discharge millions of tons of nuclear sewage generated by the Fukushima Daiichi nuclear power plant into the sea in batches [7]. The Japanese government has stated that all radionuclides, such as cesium, strontium, and cobalt, except tritium, have been removed from wastewater;

This work was supported by the National Natural Science Foundation of China (No. 12105029).

✉ Qing-Xian Zhang
shinecore@163.com

¹ Chengdu University of Technology, Chengdu 610059, China

however, the discharge of tritium into the ocean will affect global fish migration, pelagic fisheries, human health, and ecological safety. Therefore, monitoring tritiated water activity is vital for research purposes as well as for protecting human health.

Liquid scintillation is typically performed to measure the activity of liquid tritium in nuclear power plants [8]. It involves pretreating a tritiated water sample to be measured to eliminate the effects of organic matter and other radionuclides on the measurement results. Subsequently, the treated tritiated water sample and scintillation solution are mixed in a certain ratio, agitated equally, and placed into a liquid scintillation analyzer to measure the activity of tritium in water after a certain duration [9, 10]. The lower limit of liquid scintillation measurement can be as low as 0.5 Bq/L; however, liquid scintillation presents some disadvantages. To perform measurement, the type of scintillation solution must be selected based on the specific situation, and the scintillation bottle, amount of scintillation solution, sample pretreatment, and standing time will affect the measurement results [11, 12]. Performing liquid scintillation to measure the activity of tritium in water will cause the scintillation solution to become radioactive organic liquid waste, thus causing secondary contamination to the environment. The period for measuring radioactivity in liquids using the liquid scintillation method is approximately three days; therefore, real-time online monitoring of tritium activity in liquids is not realizable. The International Bureau of Weights and Measures is developing a liquid scintillation system (ESIR) based on three simultaneously operating photon-counting channels to assess the equivalence of the primary standards for tritium, and the metrological traceability of tritium is currently being investigated. The new ESIR can deliver accurate comparison values for ^3H , ^{55}Fe , ^{63}Ni , and ^{14}C , and is not affected by changes in the detection efficiency or asymmetry of the counting channels [13].

In 2015, Florian Priester of the Karlsruhe Institute of Technology in Germany fabricated a detector for measuring tritiated water using scintillating fibers [14]. The operation of the detector involves the energy deposition of low-energy β -rays in tritiated water into plastic scintillating fibers to generate scintillation photons. The generated scintillation photons approach the photomultiplier tubes (PMTs) at both ends through the fibers, and the PMTs convert the optical signals into electrical signals. Measurements performed using the detector do not require the preparation of measurement samples, do not generate radioactive waste, and can be reused. However, owing to the few scintillating fibers, relatively crude detector design, and relatively high electronics noise, we were able to conduct only online measurements of liquid tritium activity at 10^7 Bq/L by 2019 after performing continuous

improvement [15]. Here study is based on the measurement of scintillating fibers, and we plan to improve the detection efficiency by increasing the number of scintillating fibers. The detector was composed of 241 equal-length scintillating fibers arranged in parallel intervals, which allowed tritiated water to circulate in the scintillating fibers; meanwhile, the photoelectric conversion devices acquired scintillation photons at both ends of the fiber arrays. Results from Geant4 simulations revealed that the range of β -rays from tritium decay in plastic scintillators was less than 5 μm , and that most commercial plastic scintillating fibers possess a cladding layer measuring 2–3% of their diameter, which wraps the inner plastic scintillating fibers to minimize scintillation photon spillover. The β -rays generated by the decay of tritiated water cannot penetrate even the outer cladding of scintillating fibers with a diameter of 0.5 mm, which is the smallest diameter available hitherto. Scintillating fibers are composed of cladding and an internal media; currently, only Saint-Gobain manufactures commercial plastic scintillating fibers without cladding (model BCF-10). However, those fibers are expensive and require numerous orders; additionally, owing to trade blockade by the USA, these fibers are embargoed and cannot be purchased in China. Hence, we propose a technical solution for drilling a dense array of through-holes in a cylindrical plastic scintillator and for increasing the number of circulation channels for tritiated water through the holes such that the contact area of tritiated water with the detector can be increased. This method requires less cost compared with using scintillating fibers, and the assembly process is relatively simple. Figure 1 shows an illustration and photographs of the detector.

2 Detector design

2.1 Feasibility verification

Before designing the detector, we performed two experiments to verify the feasibility of the scheme. Because we performed plastic scintillator drilling instead of fiber array scintillating, and the plastic scintillator material used is rare, the physical rigidity of the plastic scintillator was between that of ordinary plastic and glass. Previously, we discovered that some corners of the plastic scintillator were damaged after it collapsed due to gravity (the upper section of the plastic scintillator shown in Fig. 1b was damaged due to the collapse). Therefore, in our first experiment, we verified the feasibility of drilling holes in plastic scintillators. We contacted a team that conducted research on plastic scintillators [16] to borrow a 5-cm-diameter cylindrical plastic scintillator to verify its feasibility for drilling, as shown in Fig. 1b (the bubbles in the plastic

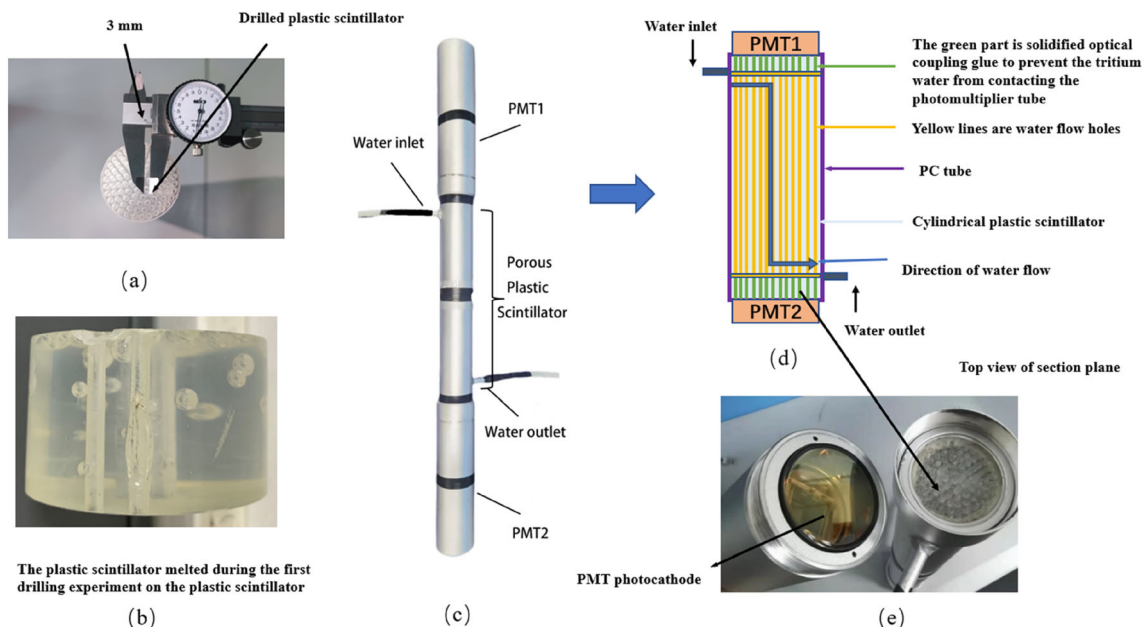


Fig. 1 (Color online) **a** Diameter of the plastic scintillator hole; **b** edge fragmentation of the plastic scintillator; **c** appearance of the detector; **d** internal model structure of the detector; **e** photograph showing one end of the photomultiplier tube and plastic scintillator

scintillator are defective products in the experimental stage). In the first drilling, the drilling speed was extremely high, and no cold water was sprayed for cooling, which resulted caused the plastic scintillator to melt owing to its low melting point. In the subsequent drilling, we reduced the drilling speed, used cold water spray for cooling, and successfully drilled the plastic scintillator. After the drilling was evaluated by a process personnel, we used a five-axis computerized numerical control (CNC) machine tool to punch holes in both directions, which resulted in a minimum hole diameter of 1.5 mm and a maximum hole length of 60 cm. Figure 1c shows a photograph of the detector, and Fig. 1d shows internal model structure of the detector.

Because of the low-energy β -rays generated by the decay of tritiated water, less energy is deposited in the plastic scintillator, resulting in relatively few scintillation photons generated. The probability that the few scintillation photons propagating through the plastic scintillator being captured simultaneously by the PMTs at both ends is much lower, and the quantum efficiency of the PMTs is lower as well. Consequently, the amplitude of the captured tritiated water decay signal is small, which renders it easily concealed by the dark current of the PMTs. Therefore, we utilized two PMTs to perform coincidence measurements at both ends of the plastic scintillator. A photograph of the plastic scintillator coupled with the PMT is shown in Fig. 1e. Because the dark current of the PMTs is generated randomly and the scintillation photons generated by the β -rays of tritiated water decay propagate in the plastic

scintillator toward both ends, one can assume that scintillation photons will reach the photocathode of the PMT simultaneously and then be captured. All coincidence measurements can accurately capture the effective coincidence signal in the interspersed dark-current noise. However, in practice, the dark current generated by the PMT at both ends may be simultaneously captured by the PMT photocathode, which results in a false coincidence event. Experiments must be performed to evaluate the effect of the false coincidence count of the dark current of the two PMTs during long-term operation on the measurement results. The two PMTs were operated normally under shading conditions with their photocathodes uncoupled to any scintillator, and the dark current was observed over a long duration in accordance with the count. In the long-term measurement, when the two PMTs were operating at a high voltage of 1200 V, the dark-current coincidence count was less than 1 for 30 min. The feasibility of our detector scheme was preliminarily verified via two experiments.

2.2 Geant4 simulation

After experimentally verifying the feasibility of the detector scheme, we developed a detector model using the Geant4 software to simulate the processes of energy deposition and scintillation photon transmission to further verify the feasibility of the detector structure.

The simulation via Geant4 (using G4EmLivermorePhysics, which includes electromagnetic processes such as tough radiation, Coulomb scattering, and

fluorescence effects) showed that the deposition process of low-energy β -rays generated by the decay of tritiated water in plastic scintillators yielded scintillation photons. Additionally, the photon propagation model (using the optical physics function in Geant4) showed that scintillation photons propagating in plastic scintillators finally reached the PMT photocathode. The optical properties of water were obtained from the materials library in Geant4, whereas the properties of plastic scintillators were obtained from the Geant4 NIST database G4_POLYSTYRENE [17]. Meanwhile, the parameters of the plastic scintillator were obtained from the manufacturer (refractive index, 1.58; density, 1.05; hydrocarbon ratio, 1:1.1; decay time, 2.4 ns; scintillation photon decay length, 2.44 m), and a photon yield of 12,250/MeV provided by the manufacturer was applied without considering the possible nonlinearities at low energy [18].

Figure 2a shows the simulated range of the β -rays generated by tritium decay in water and plastic scintillators. As shown, the range in both water and plastic scintillator does not exceed 5 μm , which implies that the β -rays generated by the decay of tritiated water beyond 5 μm from the plastic scintillator do not contribute to the measurement

results. Only the β -rays generated by tritiated water decay within 5 μm of the plastic scintillator can deposit energy in the plastic scintillators. In the Geant4 simulation, the emission position of the β -particles was set in the tritiated water layer within 5 μm from the surface of the plastic scintillator after drilling, and the emission direction of the β -particles was isotropic. The number of particle incidences in each simulation was set to 100 million to ensure the convergence of the Monte Carlo simulation. Only the β -rays generated by the decay of tritiated water within 5 μm from the surface of the plastic scintillator can be incident on the plastic scintillator to deposit energy and then be detected. To achieve online measurements of low-activity tritiated water, a sufficiently large contact area must be ensured between tritiated water and the surface of the plastic scintillator to allow an adequate amount of β -rays to be incident on the plastic scintillator per unit time. Because the maximum diameter of the typically used PMT manufactured by Hamamatsu is 5.1 cm, its price is the most cost-effective comparatively. Furthermore, because the price of a PMT with a diameter exceeding 5.1 cm has increased rapidly, we decided to use a cylindrical plastic scintillator with a diameter of 5 cm. The maximum length

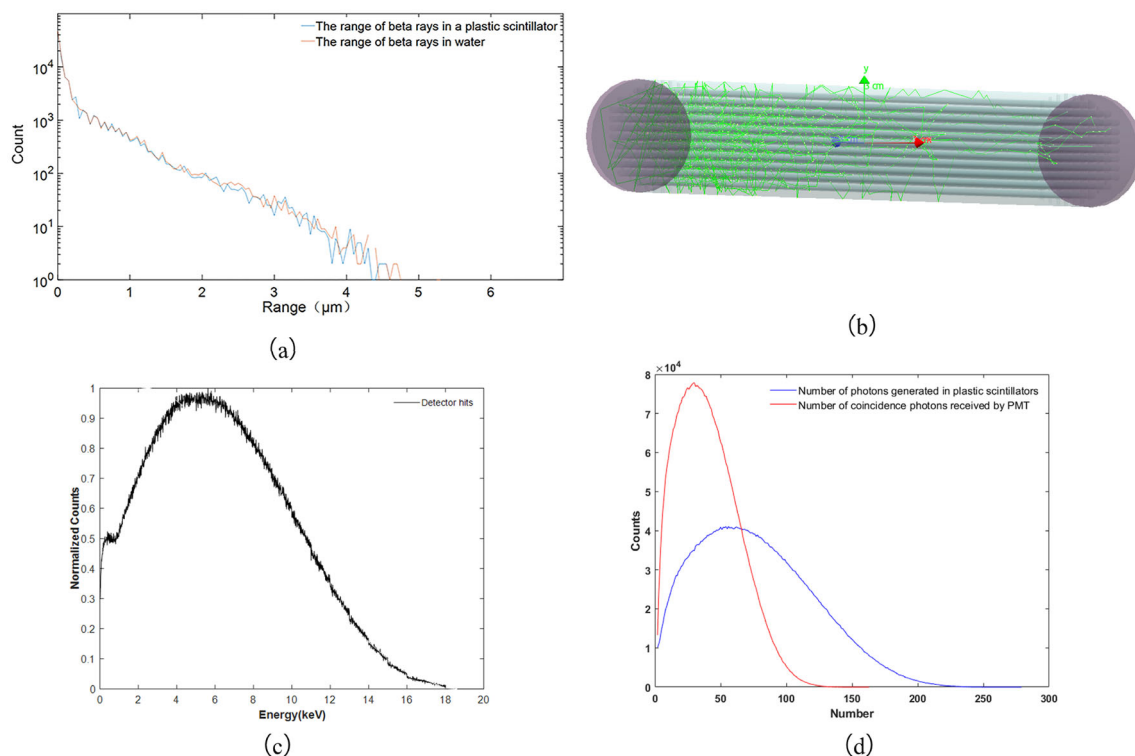


Fig. 2 (Color online) **a** Range of β -rays generated by decay of tritiated water in water and plastic scintillators. **b** Propagation process of scintillation photons in detector generated by β -rays during decay of tritiated water (green curve shows propagation path of the scintillator photons). **c** Normalized energy spectrum of β -ray deposited energy in the plastic scintillators. **d** Number spectrum of

photon; blue curve shows scintillation photon spectrum produced by β -rays inside the plastic scintillator, and red curve shows spectrum of coincidence photons received simultaneously at both ends of the PMT, where the abscissa and ordinate represent the number of photons and the number of times that number appears in all simulations, respectively

of the plastic scintillator borehole evaluated by the processing master during drilling was 60 cm; therefore, when the length of the plastic scintillator was 60 cm, the effective volumes were calculated for hole diameters of 1, 2, 3, 4, and 5 mm. When the hole spacing was 1 mm, the effective volumes of β -rays generated in tritiated water that can be incident on the plastic scintillator were 0.0050, 0.0051, 0.0034, 0.0032, and 0.0024 L, respectively, for the abovementioned hole diameters. The effective volume was the largest when the aperture was 2 mm. However, considering that a hole diameter of 3 mm (compared with the other diameters above) is easier to achieve in both directions using a five-axis CNC machine when the length of the plastic scintillator is 60 cm, we used a hole diameter of 3 mm in the simulation of Geant4 and in the actual processing of the detector at a later stage.

Figure 2b shows an effective example of the energy deposited in the plastic scintillator by β -rays generated via tritiated water decay, as simulated in Geant4. The scintillator photons were propagated in the plastic scintillator and captured simultaneously by the PMT photocathodes at both ends. Figure 2c shows the normalized energy spectrum of the β -ray energy deposited in the plastic scintillator. The peak of the β -ray energy spectrum from the decay of tritiated water was approximately 3 keV, and the average value was 5.7 keV, whereas the peak of the β -ray energy deposited in the plastic scintillator was approximately 6 keV, as shown in Fig. 2c. The energy peak shifted to the right because some of the relatively low-energy (Left side of the peak) β -rays have lost all their energy before they were incident on the plastic scintillator. Based on a model with a plastic scintillator diameter of 5 cm and a length of 60 cm, we drilled a dense array of holes featuring a diameter of 3 mm and a spacing of 1 mm parallel to the axis. We simulated the number of scintillation photons generated by the β -rays in the plastic scintillator and the number of coincidence photon curves received at both ends of the PMT, as shown in Fig. 2d. Based on the curve, the deposition energy of β -rays in the plastic scintillators and the number of coincidence photons arriving at both ends of the PMT decreased owing to the material self-absorption effect and other factors. We simulated 100 million β -particles emitted in tritiated water within 5 μm from the plastic scintillator surface, and the number of events in which no less than one photoelectron was captured simultaneously by the PMT at both ends was 3,735,924 (the quantum efficiency of the PMT was considered in the Geant4 simulation, and the quantum efficiency graphs were obtained from the PMT manufacturer). In other words, the detection efficiency of this detector (60 cm long) was approximately 3.74% for the effective β -ray emission volume (5 μm water layer). Using this data, we can calculate the number of pulses detected per unit time based on

the activity of the β -rays. When the length of the cylindrical plastic scintillator was changed but its diameter, number of holes, and aperture were fixed, the detection efficiency for the effective β -ray emission volumes was 3.74%, 3.84%, 3.94%, 4.06%, and 4.19% at lengths of 60, 50, 40, 30, and 20 cm, respectively. Although the detection efficiency increased gradually as the detector length decreased, the peak position of the coincidence photon spectrum shifts to the right with decreasing detector length (i.e., the average amplitude of the detector output signal decreases with increasing length, and the signal-to-noise ratio (SNR) of the back-end electronics was required). However, because of the large contact area between the 60-cm-long detector and tritiated water, more β -rays for depositing energy were incident on the plastic scintillator; therefore, the detector length was specified as 60 cm. By selecting a low-noise PMT and designing high SNR electronics, amplitude reduction in the output signal caused by the long-distance propagation of scintillation photons is overcome.

Next, the reliability of the detector model and the feasibility of the design solution were verified. The final detector model was a 5-cm-diameter cylindrical plastic scintillator with a dense array of through-holes drilled parallel to the axis, where the hole diameter and spacing were 3 and 1 mm, respectively, and the length of the cylindrical plastic scintillator was 60 cm.

2.3 Detector construction

The entire detector unit was classified into three regions: the middle region comprised the plastic scintillator and sealed alloy housing, and the two ends comprised the PMT and sealed housing.

Tritiated water flowed through the water inlet of the detector and passed through the water outlet after passing through the plastic scintillator. During the flow of tritiated water in complete contact with the scintillator detector, the β -ray emitted by the decay was launched toward the plastic scintillator to deposit energy and generate scintillation photons. The scintillation photons propagated in the plastic scintillator and water and finally reached the PMT to be converted into photoelectrons and formed a pulse signal. Because the refractive index of the plastic scintillator is higher than that of the surrounding water, most of the photons generated inside the plastic scintillator will remain therein owing to total reflection. Therefore, a polycarbonate (PC) tube and a 1.5-cm-thick alloy housing were used to construct the detector housing. The PC tube can reflect some of the scintillation photons that escape from the cylindrical plastic photons, and its mechanical processing performance is favorable for drilling. Meanwhile, the 1.5-cm-thick alloy shell can obstruct the external β -rays. The

PMT was fabricated using R6231-100, which contains potassium-free borosilicate glass (low dark current) and features a high electron multiplication gain and high quantum efficiency. The R6231-100 housing was fabricated using permalloy to reduce the effects of the geomagnetic field.

As inlets and outlets for the flow of tritiated water, 15-mm-diameter holes were drilled at both ends of the detector housing; meanwhile, transverse holes were drilled in the plastic scintillator parallel to the upper and lower circular surfaces in the transverse position of the tritiated water inlets and outlets. The ends of the plastic scintillator near the PMT were filled with solidifiable optical coupling adhesive to prevent direct contact between the tritiated water and the PMT photocathode. Teflon tape was used to seal the ends of the plastic scintillator and to shield the housing.

3 Electronics design

For the online measurement system for low-activity tritiated water developed in this study, we designed a back-end electronic system, the principle framework of which is shown in Fig. 3.

A design margin was implemented in the entire circuit system to accommodate additional detectors and functions in the detector system in the future [19, 20]. Because the

rising edge of the plastic scintillator output signal was only a few nanoseconds wide, an OPA657 chip with a maximum -3 dB bandwidth of 1.6 GHz was selected. Transimpedance amplification yielded by a transimpedance circuit converts the current signal from the PMT output into a voltage signal while preserving the original waveform shape of the signal and reducing the possibility of signal accumulation [21]. The transimpedance amplifier circuit was integrated on the same circular circuit board as the resistive divider circuit required by the PMT. It was located immediately at the output of the PMT to reduce parasitic capacitance and improve the SNR, whereas the input was isolated by a protection ring to reduce the effect of leakage current on the signal. The signal amplified by the operational amplifier (op-amp) at both ends of the PMT was transmitted to the data acquisition board at the back-end via the same cable used for signal transmission. The first-stage op-amp of the data acquisition board can realize gain adjustment during signal amplification while achieving impedance matching. The gain adjustment command from the host computer is transmitted to the field-programmable gate array (FPGA) of the data acquisition board, and the FPGA realizes the change in resistance of the amplifier circuit by controlling the opening and closing of different paths of the ADG611, thus realizing controllable gain adjustment. The second-stage op-amp transforms the single-ended signal into a differential signal and inputs it into a high-speed analog-to-digital converter (ADC) with

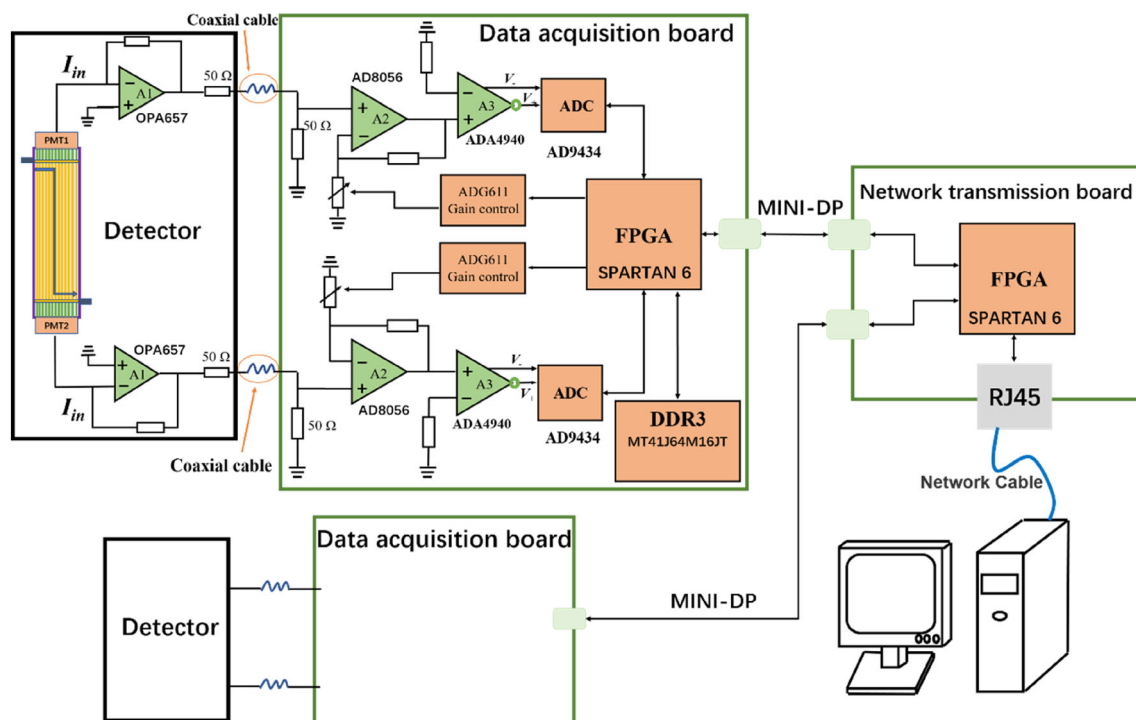


Fig. 3 Electronics design framework for low-activity tritiated water online measurement system

a sampling rate of up to 500 MSPS. The FPGA acquires and packages data from two ADCs and then assesses the FPGA. The FPGA transmits the amplitude and timestamp of the two signals, which are coincident simultaneously (at 50 ns, which conforms to the time window), to the back-end network transmission board via a MINI-DP interface. The network transmission board is a gigabit network transmission module, whose main function is to transfer data from the data acquisition board to the upper computer at the back end. The most significant advantage of the entire electronic system is its expandability, which is reflected in the structure. An upper computer can link multiple network transmission boards through a router, and one network transmission board can connect multiple data acquisition boards. When a network board is connected to multiple data acquisition boards, the system clock is distributed uniformly from the network board to multiple data boards below it. The scalability of the electronics is reflected in their functionality. Because the focus of this study is on tritiated water activity measurements, only the number of coincident pulses must be considered. When the measurement background is complex, after refining or modifying the detector system, different rays may need to be filtered by different amplitudes or waveforms. The data acquisition and network transmission boards have separate FPGAs, which ensures sufficient resources to perform complex logic judgments on-chip. Furthermore, a 1 Gbit double-data-rate three synchronous dynamic random access memory (DDR3) chip was implemented in the data acquisition board to prevent data blockage. When the detector structure composition is changed at a later stage, the waveform signal that occurs simultaneously must be transmitted to the host computer to identify and distinguish α - and β -rays using the waveform information. In a system transmission rate test, we used 1111–1111 as the seed and 1011–0001 as the feedback coefficient to generate an 8-bit

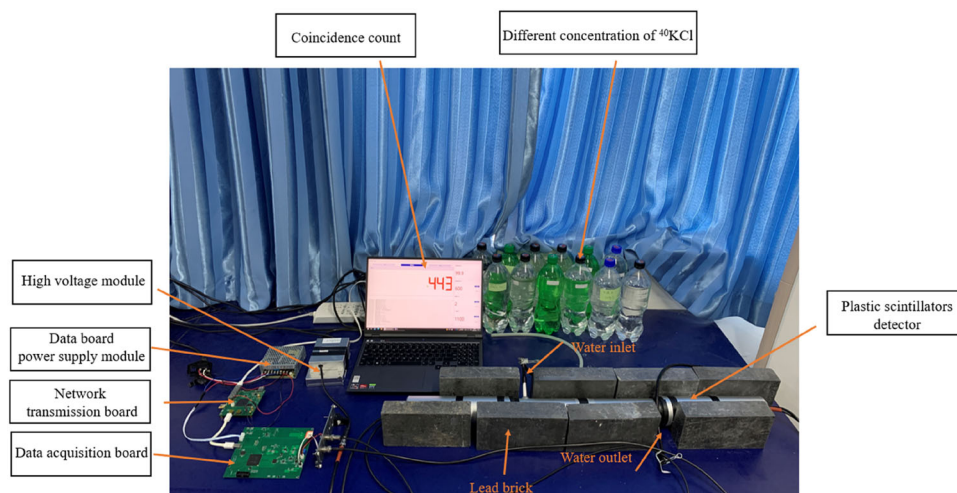
pseudo-random number in the linear feedback shift register of the FPGA of the data acquisition board. Subsequently, the number was transmitted to the host computer through the network board. The transmission clock frequency of the MINI-DP was 500 MHz, and the received pseudo-random numbers were verified in real time on the host computer to obtain the transmission rate and bit error rate (BER). We performed the test continuously for 28 h and discovered that the transmission rate of the MINI-DP was stable at approximately 30.5 MB/S (a gigabit network provides the transmission rate of bits in terms of gigabits, not bytes), with a BER of 0. All the electronics were designed to allow functional and structural expansion of the detector system at a later stage.

4 Experiment

4.1 Test platform

Because tritiated water is strictly controlled and difficult to obtain, we used a potassium chloride solution instead as the solution to be measured in our experiment. K-40 is a radioactive isotope of potassium that decays and emits β - and γ -rays. The maximum energy of β -rays is 1.31 MeV, and the maximum energy of β -rays generated by the decay of tritiated water is only 18.6 keV. Therefore, a controlled amplification adjustment function was added to the electronics design. An ADG611 chip, which was controlled by the FPGA, was used to adjust the amplification of the op-amp such that compatible measurements of potassium chloride and tritiated water can be achieved. The abundance of K-40 in the potassium solution was 0.0117%. Because the solubility of potassium chloride at 20 °C is 34.2 g, based on the purchased potassium chloride with 99.5% purity, we prepared the following 13 activities for

Fig. 4 (Color online) Experimental measurement platform constructed using detector system



the potassium chloride: 10, 50, 100, 200, 500, 1000, 1500, 2000, 2500, 3000, 3500, and 4000, and 4500 Bq/L.

Figure 4 shows the test platform for this experiment, which comprises a shield, plastic scintillator β -ray detector, high-voltage module, data acquisition board, network transmission board, power supply module, and PC.

The shield shown in Fig. 4 is a lead brick, which was not used as a shield in the final measurement. We used lead-brick shields to determine the effect of external background radiation on the total count. In the later tests, we discovered that the background counts per unit time were stable in the long term; therefore, we stopped using lead-brick shields in the subsequent experimental measurements.

The power supply used in the system was a Meanwell switching power supply, which provides a + 12 V output and a \pm 5 V output to power the high-voltage module and electronics, respectively. The high voltage was provided by Wiseman’s controllable high-voltage module, and the high-voltage output was directly controlled and monitored through the PC terminal. Both PMTs used the same high-voltage power supply since both were fabricated in the same batch, and their relative deviation was insignificant (based on factory testing). A voltage of \pm 5 V was used to supply power to the data acquisition and network transmission boards.

4.2 Linear measurement

The PMT was operated at 1000, 1050, 1100, 1150, 1200, 1250, 1300, and 1350 V. The trends of the measured

counts with respect to the activity of the solution are shown in Fig. 5.

As shown Fig. 5, the count for the same activity increases gradually with the voltage. At the same high-voltage value, a linear fit was performed using the least-squares method for the 13 different activity values, and the goodness of fit (R^2) increased and then decreased as the high voltage increased. The best R^2 was 0.9994 when the high voltage was 1300 V. The difference between the ideal fitted and actual measured values is reflected by the relative deviation, $R_\sigma = \frac{D_{act}-D_{ideal}}{D_{ideal}} \times 100\%$, where D_{act} is the actual measured value, and D_{ideal} is the ideal fitted value. We obtained maximum relative deviations of 14.99%, 12.40%, 24.46%, 3.21%, 13.94%, 7.49%, 5.16%, and 11.90% for 1000, 1050, 1100, 1150, 1200, 1250, 1300, and 1350 V, respectively. When the detector was operated at 1300 V, the linear R^2 was the best, and the maximum relative deviation and counts per unit time were sufficient. Therefore, based on our experiments, the optimal operating voltage of the detector for measuring the KCl solution was 1300 V. When the detector was operated at 1300 V, the average count of the highest-concentration KCl solution was 74,542 per 10 min, with coincidence pulses at approximately 124 pairs per second. Because the electronics contained a 1 Gbit DDR3 chip, the maximum effective transmission rate of the back-end network transmission board was 30.5 MB/S, which can be realized by the electronic system even if a full sampling of the coincidence waveform is transmitted at a later stage. Therefore, the operating high voltage of 1300 V not only guarantees the favorable linear R^2 of different solution activities, but also ensures that the counting per unit time will not result in a system dead time.

To investigate the effects of different measurement times, the high voltage was set as 1300 V, and the results were examined for measurement times of 10, 20, 30, 40, 50 and 60 min, as shown in Fig. 6.

As shown in Fig. 6, the linear R^2 exceeds for the measurement time from 10 to 60 min when the operating high voltage is 1300 V. At different measurement times, we obtained maximum relative deviations of 5.98%, 5.93%, 5.92%, 5.67%, 5.49%, and 5.16% for 10, 20, 30, 40, 50, and 60 min, respectively. Furthermore, we discovered that the maximum relative deviations from 10 to 60 min were sufficient, the overall trend was positive, and the maximum relative deviation of the counts at 60 min was the smallest. The linear R^2 increased gradually as the measurement time was extended; however, the maximum R^2 was recorded at 50 min, which was maintained even when the measurement time was further increased to 60 min. As shown in Figs. 5 and 6, the measurement count for 10 min was counted when the operating high voltage was 1300 V; the

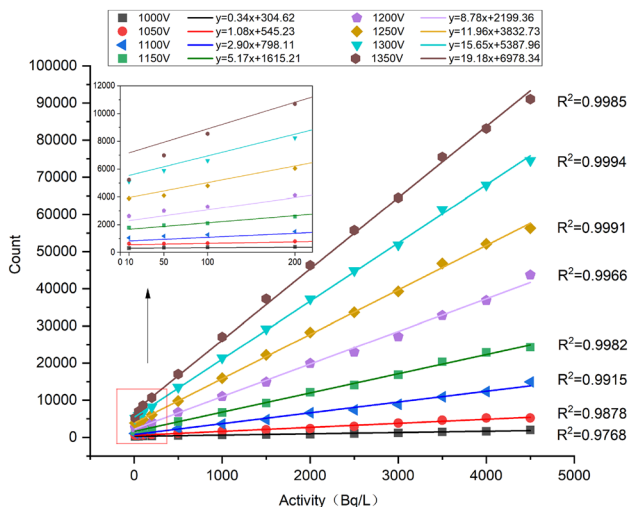


Fig. 5 (Color online) Count vs. activity for the same measurement time and different operating high voltages. Total count was read every 10 min. Each activity solution was read six times continuously at a certain high voltage, and the average value of the six counts was regarded as the count value of solutions with different activities at that high voltage

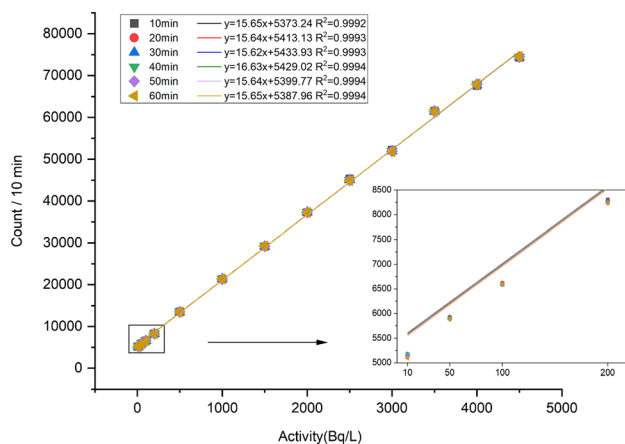


Fig. 6 Count vs. activity for the same operating high voltage and different measurement times. Total counts for different measurement times were converted to average counts over a 10-min period, e.g., the 60-min count is in fact the total count over 60 min divided by 6

linear R^2 was observed to be higher than that for the counting effect of 60 min under other operating high voltages. This test shows that a suitable operating high voltage can significantly reduce the measurement time without affecting the system's measurement results, which is a significant advantage of online measurement systems.

4.3 Stability measurement

To test the stability of the detector system, we operated the detector at 1300 V and measured the change in counts per 10 min for two cases: air and 2000 Bq/L potassium chloride solution in the detector. As shown in Fig. 7, each case was measured for seven days, and 1008 counts in units of 10 min were obtained. Figures 7a and c shows the variation in counts per 10 min with time for both measurement cases. Figures 7b and d shows the Gaussian fits of the counts at each 10-min measurement time for the two measurement cases. The average counts \bar{x} per 10 min for air and the 2000 Bq/L ^{40}KCl solution were 1938 and 37,261, respectively, and their standard deviations S were 51.948 and 372.037, respectively. Based on the relative deviation formula $\frac{S}{\bar{x}} \times 100\%$, the relative deviations were 2.68% and 0.998%, respectively, and the Gaussian R^2 values were 0.9640 and 0.9849, respectively. The relative deviations of air and the 2000 Bq/L potassium chloride solution per hour were 1.71% and 0.854%, respectively, which are lower (i.e., better) than those obtained by counting every 10 min.

5 Summary

In this study, an online detector system based on plastic scintillators was designed to monitor the activity of tritiated water in the liquid effluents of nuclear power plants. The feasibility of the detector was verified through simulations using Geant4. Based on the results of the Geant4 simulation and the actual industrial processing level, the optimal detector structure size was determined; subsequently, the detector was fabricated. A two-terminal PMT coincidence measurement mode was used in the detector to reduce the effect of dark-current noise on pulse counting. A dual-channel high-speed analog-to-digital conversion circuit was designed for the detector used in two PMT coincidence measurements. The coincidence measurements were performed on an FPGA in the data acquisition board, which directly transmits valid coincidence signals to the back-end PC for data processing. In addition, it significantly reduces the amount of data transferred from the data acquisition board to the back-end PC via the network transmission board in the actual measurements. An experimental measurement platform of β -rays based on a ^{40}KCl solution was constructed to measure 13 ^{40}KCl solutions of different activities ranging from 10 to 4500 Bq/L. The optimal PMT operating high voltage was determined to be 1300 V, and a linear fit was performed using 10-min counts. Consequently, maximum linear R^2 values of 0.9992 and 0.9994 were obtained until the measurement time of 50 min. The long-term stability of the detector was measured for both air-filled and 2000 Bq/L potassium chloride solutions, where the relative deviation of counts per 10 min was 0.998%, and the Gaussian R^2 of counts was 0.9849 for the 2000 Bq/L potassium chloride solution.

These results of this study can be used to address the situation in which nuclear power plants cannot obtain the activity information of tritiated water in real time, and for solving problems such as liquid waste due to the measurements by the offline liquid scintillation method.

6 Outlook

In this study, the current detector system verified only the initial feasibility of measuring high-energy β -ray activity online in KCl solutions, i.e., the effects of different flow rates on counting and longer-term stability measurements of KCl solutions must be investigated in the future. After performing the flow-rate problem test, the flow rate of the liquid to be measured was fixed by adding a buffer box at the front end. The effects of liquid immersion and microorganism growth on the performance of the plastic scintillator should be investigated to determine whether the

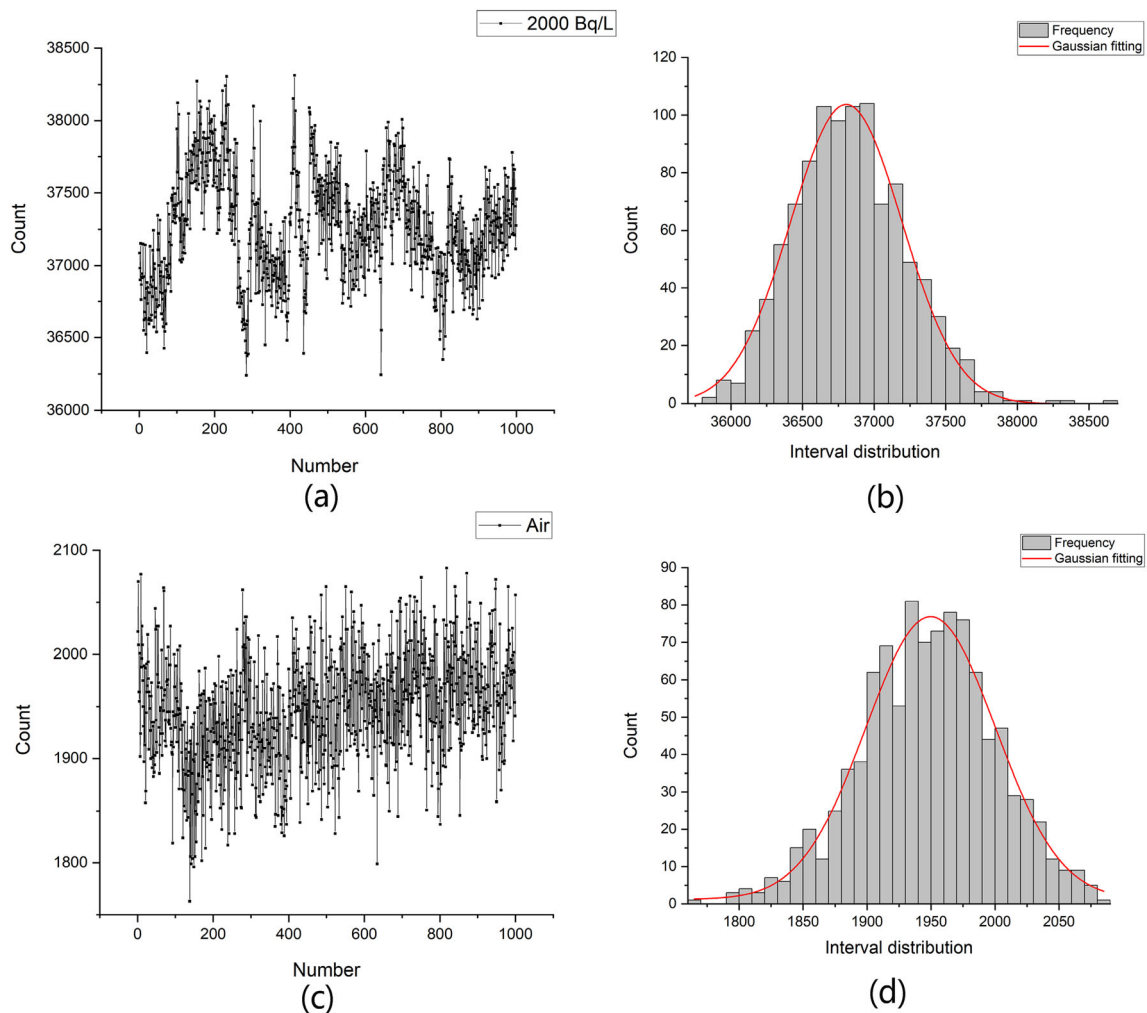


Fig. 7 Long-term stability test results of the detector system. **a** and **c** show counts per 10 min with time for KCl solution with activity of 2000 Bq/L and air, respectively, where the interval between two

adjacent points in the abscissa is 10 min. **b** and **d** show Gaussian fitting graphs of the two cases, respectively

number of water purification systems at the front end should be increased for the actual tritiated water activity measurement.

Additionally, investigations must be performed to identify whether the contributions of β - and γ -ray counts to the total counts can be distinguished more clearly based on the solution spectrum. Although a plastic scintillator is a low-Z material, the all-energy peak of its γ -energy spectrum cannot be obtained. Simultaneously, the action principle of γ -rays in the plastic scintillator is the same as that of β -rays and cannot be distinguished based on their waveforms. However, in the tritiated water measurement, the pulse amplitude caused by the low-energy β -rays generated by tritiated water was extremely low, whereas the signal amplitude generated by the background-influenced γ -rays was relatively high. Theoretically, a more accurate tritiated water activity measurement can be achieved using the solution spectrum.

Subsequently, we verified the feasibility of the system using a KCl solution and investigated the effects of different high voltages on the measurement results. However, when the system is used to measure tritiated water, the tritiated water may not be able to be measured directly by merely changing the gain of the main amplifier circuit. In the initial selection of the PMT, we focused only on the high quantum efficiency; therefore, the high gain should be considered as well in the future. Additionally, the results obtained under the highest operating voltage should be compared. We thank the reviewer for the constructive opinions and suggestions regarding future tritiated water measurements.

Finally, the method used in the system must be compared with the liquid scintillation method for tritiated water measurements to determine the optimal operating high voltage and measurement time in an actual environment.

Author contributions All authors contributed to the study conception and design. Material preparation, data collection and analysis were performed by Chun-Hui Dong., Kai-Yong Liao, and Rui-Yang Xu. The first draft of the manuscript was written by Chun-Hui Dong, and all authors commented on previous versions of the manuscript. All authors read and approved the final manuscript.

References

1. D.P. Li, Z.Q. Pan, Radiation protection handbook, 1st edn. (Atomic Energy Press, Beijing, 1990), pp. 118–120. (in Chinese)
2. Z.L. Chen, S.M. Peng, H. Chen et al., Development of a novel system for monitoring tritium in gaseous form. *Nucl. Sci. Tech.* **26**(2), 020602 (2015). <https://doi.org/10.13538/j.1001-8042/nst.26.020602>
3. L. Zhu, Radiochemistry, 1st edn. (Atomic Energy Press, Beijing, 1985), p. 315. (in Chinese)
4. H.Y. Yang, Tritium Safety and Protection, 1st edn. (Atomic Energy Press, Beijing, 1997), p. 37. (in Chinese)
5. K.J. Hofstetter, H.T. Wilson, Aqueous effluent tritium monitor development. *Fusion Technol.* **21**, 446–451 (1992)
6. F. Liu, Y.H. Li, J. Lin, A hydrogen and oxygen isotope study of groundwater in the yongding river drainage of Beijing and its environmental significance. *Acta Geosci. Sin.* **29**(2), 161–166 (2008). [https://doi.org/10.3321/j.issn:1006-3021.2008.02.005\(inChinese\)](https://doi.org/10.3321/j.issn:1006-3021.2008.02.005(inChinese))
7. D. Normile, Japan plans to release Fukushima's wastewater into the ocean. *ScienceMag.* (2021). <https://doi.org/10.1126/science.abi9880>
8. Z.G. Ren, B.T. Hu, Z.P. Zhao et al., Digital coincidence acquisition applied to portable β liquid scintillation counting device. *Nucl. Sci. Tech.* **24**(3), 030401 (2013). <https://doi.org/10.13538/j.1001-8042/nst.2013.03.012>
9. I. Jakonić, N. Todorović, J. Nikolov et al., Optimization of low-level LS counter quantulus 1220 for tritium determination in water samples. *Radiat. Phys. Chem.* **98**, 69–76 (2014)
10. C. Varlam, I. Stefanescu, O.G. Dului et al., Applying direct liquid scintillation counting to low level tritium measurement. *Appl. Radiat. Isot.* **67**(5), 812–816 (2009). <https://doi.org/10.1016/j.apradiso.2009.01.023>
11. F. Verrezen, H. Loots, C. Hurtgen, A performance comparison of nine selected liquid scintillation cocktails. *Appl. Radiat. Isot.* **66**(6), 1038–1042 (2008). <https://doi.org/10.1016/j.apradiso.2008.02.050>
12. Z.L. Chen, S.X. Xing, H.Y. Wang et al., The effect of vial type and cocktail quantity on tritium measurement in LSC. *Appl. Radiat. Isot.* **68**(9), 1855–1858 (2010). <https://doi.org/10.1016/j.apradiso.2010.04.015>
13. R. Coulon, R. Broda, P. Cassette et al., The international reference system for pure β -particle emitting radionuclides: an investigation of the reproducibility of the results. *Metrologia* **57**(3), 035009 (2020). <https://doi.org/10.1088/1681-7575/ab7e7b>
14. F. Priester, M. Klein, Tritium activity measurements with a Photomultiplier in liquids-The TRAMPPEL experiment. *Fus. Eng. Des.* **109–111**, 1356–1359 (2016). <https://doi.org/10.1016/j.fusengdes.2015.12.027>
15. F. Priester, A new device for activity measurement of tritiated water. *Fus. Sci. Technol.* **71**(4), 600–604 (2017). <https://doi.org/10.1080/15361055.2017.1289585>
16. X.B. Li, Z.H. Wang, H.W. Lv et al., Measurement of the energy of fast neutrons in the presence of gamma rays using a NaI (TI) and a plastic scintillator. *Nucl. Instrum. Meth. A* **976**, 164257 (2020). <https://doi.org/10.1016/j.nima.2020.164257>
17. M.M. Nasser, Q.-L. Ma, Z.-J. Yin et al., Monte-Carlo simulation to determine detector efficiency of plastic scintillating fiber. *Nucl. Sci. Tech.* **15**(5), 308–311 (2004). <https://doi.org/10.1088/1009-1963/13/2/003>
18. R.Y. Xu, C.H. Dong, X.Q. Mao et al., Simulation results of the online tritiated water measurement system. *Nucl. Sci. Tech.* **32**(11), 126 (2021). <https://doi.org/10.1007/s41365-021-00964-1>
19. H.-K. Wu, C. Li, A ROOT-based detector test system. *Nucl. Sci. Tech.* **32**(10), 115 (2021). <https://doi.org/10.1007/s41365-021-00952-5>
20. P. Juyal, K.-L. Giboni, X.-D. Ji et al., On proportional scintillation in very large liquid xenon detectors. *Nucl. Sci. Tech.* **31**(9), 93 (2020). <https://doi.org/10.1007/s41365-020-00797-4>
21. H. Liu, C.H. Dong, X.Y. Yang et al., A high-bandwidth low current transimpedance amplification circuit. *J. Instrumen.* **16**(11), P11032 (2021). <https://doi.org/10.1088/1748-0221/16/11/P11032>

Springer Nature or its licensor holds exclusive rights to this article under a publishing agreement with the author(s) or other rightsholder(s); author self-archiving of the accepted manuscript version of this article is solely governed by the terms of such publishing agreement and applicable law.